Nanostructured Porous Silicon-Solid Lipid Nanocomposite: Towards Enhanced Cytocompatibility and Stability, Reduced Cellular Association, and Prolonged Drug Release

*Dongfei Liu, Ermei Mäkilä, Hongbo Zhang, Barbara Herranz, Martti Kaasalainen, Päivi Kinnari, Jarno Salonen, Jouni Hirvonen, and Hélder A. Santos**

A major bottleneck in nanometer-scale drug delivery systems is the fabrication of nanocarriers with excellent stability under physiological conditions that can both efficiently encapsulate therapeutic agents and controllably release their payloads. Herein, the formation of a novel nanocomposite based on the encapsulation of thermally hydrocarbonized porous silicon (THCPSi) nanoparticles with solid lipid nanoparticles (SLNs) on a 1:1 ratio is described. The THCPSi-SL nanocomposites (THCPSi-SLNCs) are formed using a solid-in-oil-in-water emulsion solvent evaporation method. TEM and FTIR analyses prove that THCPSi nanoparticles are successfully encapsulated in the SLN matrix. The formation of the THCPSi-SLNCs alters the surface smoothness and hydrophobicity of the THCPSi nanoparticles, and also remarkably enhances their stability in human plasma. After encapsulation, the cytocompatibility of the THCPSi nanoparticles with intestinal, liver, and macrophage cancer cells is also greatly improved. A prolonged release of the model drug, furosemide, from THCPSi-SLNC is achieved, indicating that the SLN matrix successfully seals the pores of the THCPSi nanoparticles. Flow cytometry and confocal fluorescence microscopy studies demonstrates the significantly reduced cellular association of THCPSi-SLNCs with the cells comparing to bare THCPSi nanoparticles. Overall, the THCPSi-SLNCs exhibits superior suspensibility and better stability against aggregation in aqueous buffer solutions, increases the particle surface smoothness and cytocompatibility, reduces the cellular association, increases the in vitro stability in human plasma, and prolonges the drug release. These results suggest that the nanocomposite is a promising nanovector system for drug delivery applications.

1. Introduction

After the inadvertent discovery of porous silicon (PSi) by Uhlir at the Bell Laboratories over 50 years ago, PSi has been widely used in biomedical applications.[1] The attractive properties of PSi nanoparticles, such as large surface area and pore volume,[1–4] high loading efficiency,[1–3] biocompatibility,[5–8] and biodegradability,[6–10] make them versatile carriers for drug delivery and imaging applications.[1,4,9] Benefiting from these advantages, a wide variety of therapeutic and imaging agents have been successfully loaded into the PSi carriers, e.g., conventional drug molecules,[2,11–13] peptides,[10,14] small interfering RNA,[15] and quantum dots.[9]

High loading degree in nanostructured porous materials is only one of the basic requirements for the drug delivery systems.[3,16] The loaded therapeutic agents should also be retained and protected within the porous nanostructure before reaching the targeted sites to maximize their treatment and/or imaging efficacy, and minimize their toxicity,[17] particularly in cancer treatment. In order to achieve efficient drug delivery to the tumor cells after intravenous administration, the nanocarrier must transport the drug in the blood stream without major leaks.[18] In addition, it is imperative that the nanocarriers are somehow sheathed when moving in the blood stream to effectively escape the reticuloendothelial system (RES) screening and capture by the liver and spleen, thus prolonging the blood circulation time of the nanocarriers.[19] Only after fulfilling the above two basic requirements, the cancer targeting drug delivery system can give rise to high therapeutic efficacy with low side effects.[18]

The loading of cargos into PSi particles by electrostatic interactions and/or physical adsorption is easily achieved,[3] but due to the freely accessible pores of PSi,[20] they can be disrupted by metabolites/ions existing in the body fluids, leading to premature release of the cargos and even inactivation.[16] Efforts have been made to incorporate payloads by covalent attachment and trap cargos by oxidation within the PSi nanostructure in

D. F. Liu, H. B. Zhang, B. Herranz, P. Kinnari, Prof. J. Hirvonen, Prof. H. A. Santos
Division of Pharmaceutical Technology
Faculty of Pharmacy
University of Helsinki
FI-00014, Helsinki, Finland
E-mail: helder.santos@helsinki.fi
E. Mäkilä, M. Kaasalainen, Prof. J. Salonen
Laboratory of Industrial Physics
Department of Physics
University of Turku,
FI-20014, Turku, Finland

DOI: 10.1002/adfm.201202491

order to slow down the release rate of the loaded agents;[21] however, both of these two strategies involve chemical reactions which might result in the inactivation or degradation of the payloads.[20,22]

After intravenous administration, the fate of the nanoparticles will be partially determined by the protein–particle interactions and the formation of protein corona, which are affected by the different properties of the nanoparticles, such as composition, size, shape, surface charge, hydrophobicity/hydrophilicity, smoothness/roughness, electron transfer capability, and functional groups and targeting moieties.[23–26] Among these factors, hydrophobic and electrostatic interactions, combined with an increase in entropy caused by protein unfolding, are the main driving forces for protein adsorption.[23–26] In general, hydrophobic particles bind more to the plasma proteins than their hydrophilic counterparts.[23,25] The driving forces for protein adsorption can be dramatically reduced by coating the surface with a polymer brush that generates steric forces, such as polyethylene glycol (PEG), polyvinyl alcohol (PVA) and polyethylene oxide (PEO).[23,27,28]

Recently, we have demonstrated the in vivo and in vitro stability of radio-labelled PSi nanoparticles for imaging applications,[5,29–31] as well as the effect of hydrophobin protein coating on the biodistribution, plasma protein adsorption, and cellular interactions of the PSi nanoparticles.[29,32,33] Despite the clear improvements in the developed nanosystems, the intravenous administration of protein/polymer modified and nonmodified PSi nanoparticles have been readily recognized and cleared from the systemic circulation by the RES system.[5,29,31,34] Opsonins are usually involved in the fast clearance of the nanoparticles from the systemic circulation,[25,26] and thus, hampering an efficient delivery of the cargos to the target sites. Therefore, novel and more complex nanosystems need to emerge in order to avoid such phenomenon.

Taking this into account, we hypothesise that PSi nanoparticles encapsulated by a solid lipid nanoparticle (SLN) matrix could provide a tunable layer to seal the pores of the particles,[35–37] and thus, possibly extending the release of the payload and modulating the cellular interactions. Biodegradable SLNs prepared from lipids that remain solid at body temperature,[38] have been regarded as an alternative nanodelivery system to traditional colloidal ones.[39] The great capability of SLNs to control the release of payloads has been widely demonstrated, as well as their distinguished biocompatibility, improved bioavailability, and enhanced targeting efficiency to the brain.[38–42]

In this study, we report the successful encapsulation of hydrophobic thermally hydrocarbonized porous silicon (THCPSi) nanoparticles in a SLN matrix to form THCPSi-solid lipid nanocomposites (THCPSi-SLNCs). The successful encapsulation of THCPSi nanoparticles within the SLN matrix efficiently controlled the release of the model drug, furosemide, from THCPSi nanoparticles, altered the hydrophobicity of the THCPSi nanoparticles, and significantly improved their stability in human plasma. Furthermore, the THCPSi-SLNCs greatly reduced the cellular association with intestinal (HT-29), liver (HepG2) and macrophage (RAW 264.7) cancer cells and enhanced the cytocompatibility when compared to bare THCPSi nanoparticles.

2. Results and Discussion

2.1. Characterization of the THCPSi-SLNCs

The specific surface area of the plain THCPSi nanoparticles was ca. 210 m^2/g, the total pore volume was ca. 0.56 cm^3/g (Supporting Information Figure S1), and the calculated average pore size was ca. 10.7 nm. While the SLN matrix prevents analysis on the THCPSi pore structure after the encapsulation, the effect on the physical properties of the THCPSi nanoparticle can be assumed limited.

The FTIR spectra of SLNs, THCPSi nanoparticles and THCPSi-SLNCs are presented in **Figure 1**. The distinctive hydrocarbon related features of the THCPSi nanoparticles such as the C–H_x stretching bands around 2850–3000 cm^{-1} and various alkyl bending structures between 1250–1500 cm^{-1} are emphasized after the encapsulation into the SLN matrix. The broad absorption band at 1018 cm^{-1} is overlapped by the lipid C–O stretching vibrations, shifting the band to slightly higher wavenumbers. The presence of SLN on the surface of the THCPSi nanoparticles is confirmed by the appearance of the C–O stretching vibrations at 1730 cm^{-1}. Although the FTIR analysis confirmed the presence of the SLN matrix after encapsulation, it was not sufficient to assert whether the SLN matrix was loaded inside or coating the THCPSi nanoparticles. In order to get further insight on the structure of the THCPSi-SLNCs, complementary microscopy methods were also employed.

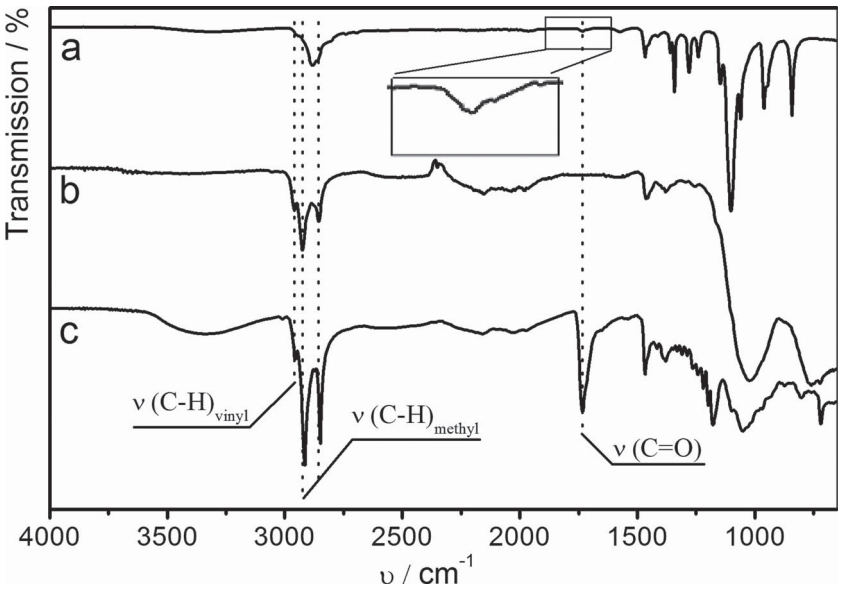

Figure 1. FTIR spectra of a) SLNs, b) THCPSi nanoparticles, and c) THCPSi-SLNCs.

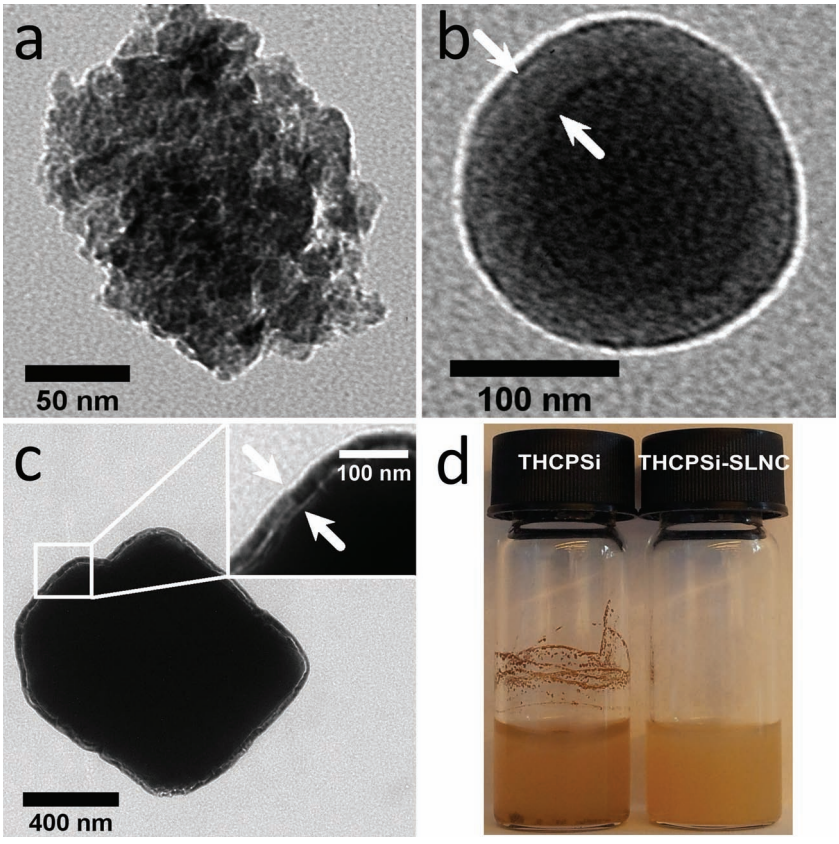

Figure 2. TEM images of the a) THCPSi nanoparticles, b) THCPSi-SLNCs, and c) THCPSi-solid lipid microcomposite, and d) the dispersion of the THCPSi nanoparticles and THCPSi-SLNCs in aqueous solution.

Since several studies have shown that inorganic particles with a size below 100 nm are internalized to a greater extent and reduce cell viability,[43,44] in order to successfully encapsulate the particles within the SLN matrix and to avoid the internalization, THCPSi nanoparticles with a size between 100 and 200 nm were prepared. The TEM images and the dispersion solutions of both THCPSi particles and their composites are presented in **Figure 2**. It can be seen that the average particle size of the THCPSi nanoparticles was ca. 150 nm (Figure 2a), whereas the THCPSi-SLNC was ca. 200 nm (Figure 2b). The particle size measured with TEM was in very good agreement with the dynamic light scattering (DLS) results (see below). Morphologically, the THCPSi nanoparticles presented a slightly irregular shape (Figure 2a). After encapsulation within the SLN matrix containing phosphatidylcholine (PC), glycerol monostearate (GMS), PVA and PEG 6000, the THCPSi-SLNCs were spherical in shape with a clear improvement in the surface smoothness (Figure 2b). Interestingly, the THCPSi-SLNC resembled a core–shell structure with the brighter SLN matrix shell surrounding the darker THCPSi nanoparticle core, formed on a 1:1 ratio (Figure 2b white arrows). The particle size of the pure SLNs prepared by the emulsion solvent evaporation method was around 200 nm (results not shown),[45] which were bigger than the THCPSi nanoparticles alone and sufficient to encapsulate these particles. As both PC and GMS are amphipathic,[46] the hydrophobic parts of these two components are likely to face inside in the THCPSi-SLNC structure and be assembled onto the hydrophobic surface of the THCPSi nanoparticles,[33] whereas the hydrophilic parts are faced towards the outer part of the THCPSi-SLNC's structure. This is further corroborated by the significant improvement in the stability and dispersibility of THCPSi-SLNCs in aqueous solutions (Figure 2d), resulting from a change in the surface hydrophobicity (turned from hydrophobic to hydrophilic).

Because of the small size of the THCPSi-SLNCs and the limited resolution of TEM, THCPSi microparticles were also employed to prepare the THCPSi-solid lipid microcomposites (ca. 3.8 μm) to distinguish the encapsulated components. TEM images showed a relatively clear "core–shell" structure composed of a THCPSi microparticle inner core and SLN matrix out-layer, forming the THCPSi-solid lipid microcomposite (Figure 2c). Due to the large size of the THCPSi microparticles, the SLN matrix is most likely to adsorb onto the surface of the THCPSi microparticles, as ascertained by the similar shape of both the THCPSi-solid lipid microcomposite and the bare THCPSi microparticle, i.e., for the THCPSi nanoparticles there is a solid lipid droplet that envelops the nanoparticle unlike the THCPSi microparticles where multiple drops accumulated and coalesced around the microparticle (Figure 2b,c). Moreover, it is also possible to observe from Figure 2b,c that the outer-layer is thicker in the case of the nanocomposite (50 nm) compared to the microcomposite (25 nm). Overall, these images indicate that the THCPSi nanoparticles were fully encapsulated in the SLN matrix and the irregular shape of the THCPSi microparticles remained unchanged after encapsulation.

2.2. Cell Viability Studies

It has been previously shown that the surface modification of the THCPSi particles can induce changes in the cytotoxic behaviour of the particles,[29,31–33,47] and the cell–nanoparticle interactions may be affected by the composition, size, shape, crystallinity, surface charge, electron transfer capability, passive targeting and the surface ligands of the nanoparticles.[24,48–50] Thus, the cytocompatibility of the THCPSi nanoparticles and the THCPSi-SLNCs with different cancer cell lines (RAW 264.7, HepG2, and HT-29) were evaluated using an ATP-based luminescent assay.[47] The cell lines were selected due to their importance as suitable models mimicking the different cell-types of the body (macrophages, hepatocytes, and mucus secreting cells) and, therefore, relevance in drug delivery applications.

All the three cell lines studied showed clear cell viabilities dependence on the particle concentrations, although these effects were less pronounced for the THCPSi-SLNCs compared

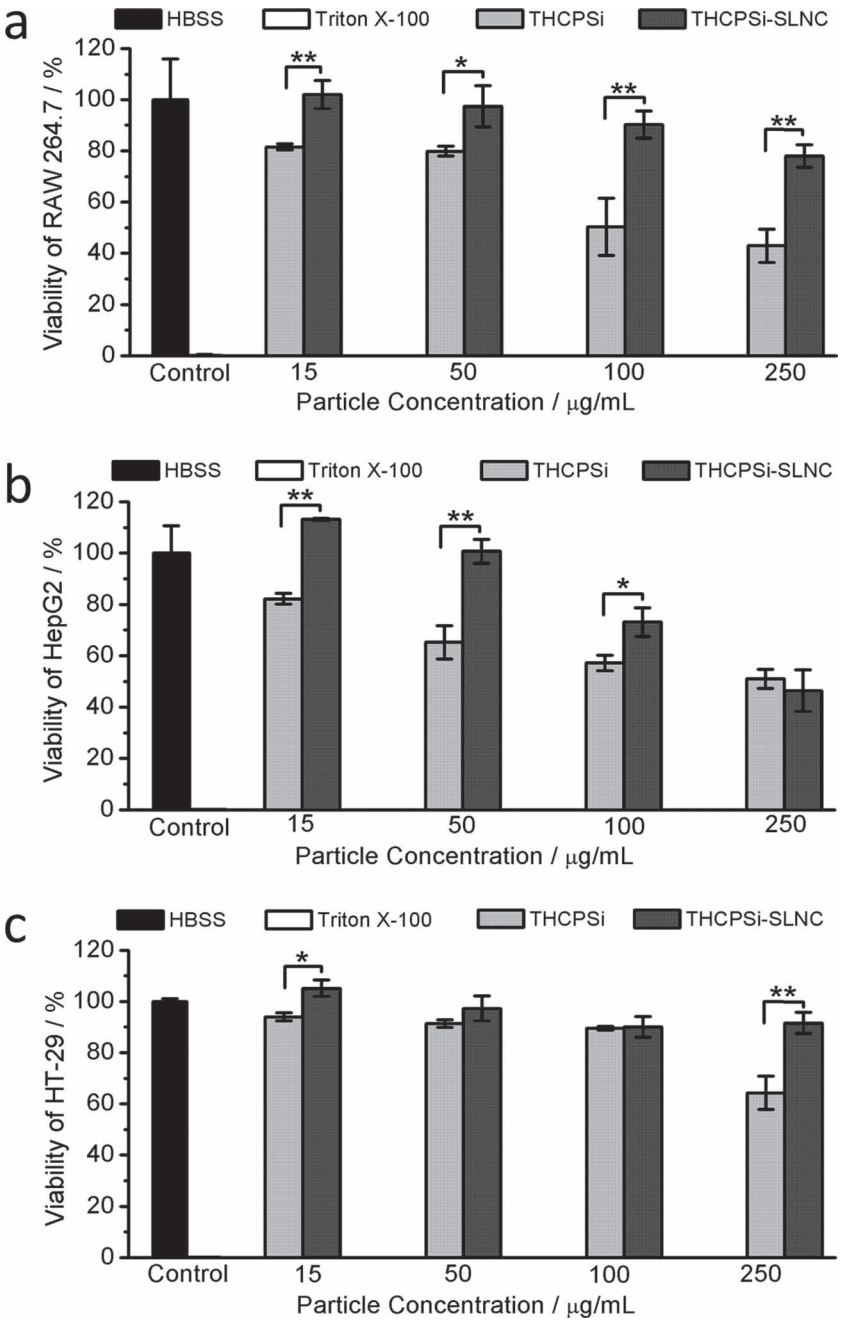

Figure 3. Cell viability of the a) RAW 264.7, b) HepG 2, and c) HT-29 cancer cells after 24 h incubation with different concentrations (μg/mL) of THCPSi nanoparticles and THCPSi-SLNCs, assessed by an ATP-based luminescence assay. Error bars represent the mean ± s.d. ($n = 3$); $^{*}p < 0.05$ and $^{**}p < 0.01$.

in cell viability of the THCPSi-SLNCs compared to bare THCPSi nanoparticles was observed for all the nanoparticle at any tested concentrations after 24 h incubation. These effects were even more pronounced at higher concentrations (100 and 250 μg/mL). Similar effects were observed for the HepG2 hepatocytes (Figure 3b), however being less evident at higher concentrations than in the RAW 264.7 macrophages. In the HT-29 intestinal cells (Figure 3c), the differences in cell viability between the THCPSi nanoparticles and the THCPSi-SLNCs were not as pronounced as in the RAW 264.7 macrophages and the HepG2 hepatocytes, but statistically significant differences were still observed between these two particles at the highest studied concentration (250 μg/mL).

Although macrophages have previously been shown to be more sensitive to the cytotoxic effects of the PSi particles due to their hydrophobic surface,[5,29,47] the cytocompatibility of the THCPSi nanoparticles was clearly enhanced within the range of concentrations studied when encapsulated within the SLN matrix (Figure 3). This could be explained by possible favourable interactions of the THCPSi-SLNCs with the cells due to the presence of biocompatible hydrophilic solid lipid[40] on the surface of THCPSi-SLNC. These interactions could be mediated by weak hydrophilic interactions of repulsive nature among the nanocomposite surface, water molecules, and the proteins of the cell membrane,[29] and thus, improving the cytocompatibility of the particles. Furthermore, the THCPSi nanoparticles were morphologically more irregular, with their shape and roughness considerably different compared to the encapsulated ones (Figure 1). Also, the different particle size compared to the THCPSi-SLNCs could also contribute for the effects observed in the cell viability studies.

Overall, the cell viability studies showed that after encapsulation of the THCPSi nanoparticles within the SLN matrix, the cytocompatibility of the nanocomposite is significantly improved compared to the bare THCPSi nanoparticles.

to the THCPSi nanoparticles (**Figure 3**). In general, the THCPSi-SLNCs promoted a statistically significant increase in cell viabilities in all the studied cell lines, in contrast to the bare THCPSi nanoparticles. The small decrease of the cell viability observed here for the cell lines studied, in comparison to previous reported data,[5,29,31,32] is probably attributed to the differences in the size/shape of the THCPSi nanoparticles. In the RAW 264.7 macrophages (Figure 3b), a significant increase

2.3. In Vitro Cellular Interactions

Based on the toxicity results, the cellular interactions of fluorescein isothiocyanate (FITC)-labelled THCPSi-SLNC and FITC-labelled THCPSi nanoparticles with RAW 264.7 macrophages, HepG2 hepatocytes and HT-29 intestinal cell lines were also assessed using flow cytometry and confocal fluorescence microscopy (**Figure 4**). The surface charge of the particles is known to

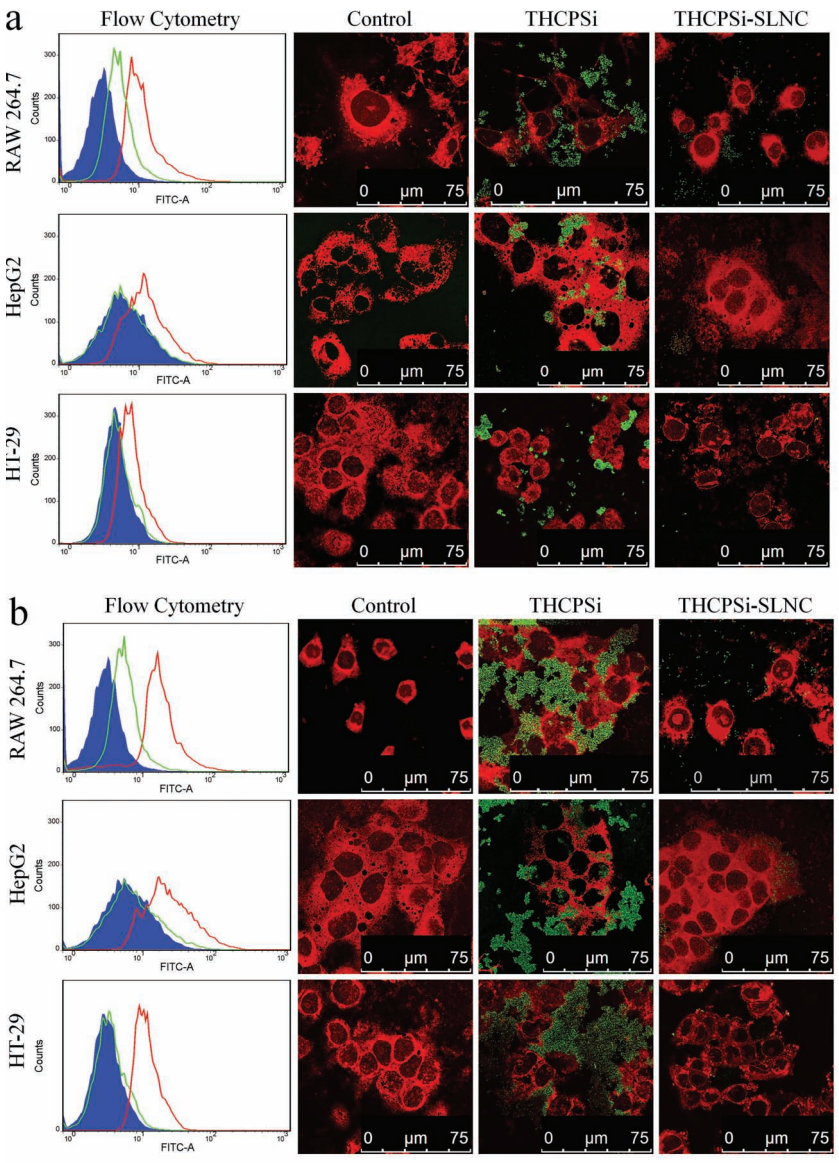

Figure 4. Flow cytometry histograms (left column) and confocal fluorescence microscopy images (right three columns) of RAW 264.7, HepG2, and HT-29 cells after 3 h incubation with FITC-labelled THCPSi nanoparticles and FITC-labelled THCPSi-SLNCs at 37 °C (scale bars = 75 µm; $n \geq 2$). Flow cytometry histograms show the fluorescent intensity of control cells (blue solid peak), cells incubated with FITC-labelled THCPSi nanoparticles (red lines) and FITC-labelled THCPSi-SLNCs (green lines). The plasma cell membranes were stained with CellMask (in orange) and were incubated with a) 50 and b) 100 µg/mL of FITC-labelled particles (in green).

play a crucial role in cell association or internalization, where positively charged particles are internalized/associated in a greater extent than negatively charged ones.[51] The extent of the cellular association of the studied particles was analyzed with flow cytometry after 3 h incubation (Figure 4, left column). Similar results were also obtained for 24 h incubation (results not shown). An increase in the cellular associated fluorescence was observed for all the cells studied when exposed to THCPSi nanoparticles. The flow cytometry histograms for THCPSi-SLNCs showed no pronounced increase in the cellular associated fluorescence for HepG2 and HT-29 cells, and only a slightly increase for RAW 264.7 macrophages. This indicates that no major association took place between the THCPSi-SLNCs and the cells under the studied experimental conditions. The normalized geometric mean values obtained from the flow cytometry histograms for the RAW 264.7 macrophages displayed ca. five-fold increase in the cellular associated fluorescence of the THCPSi nanoparticles regardless of the concentration compared to the THCPSi-SLNCs; ca. eight- and seven-fold increase in the cellular associated fluorescence of the THCPSi nanoparticles at 50 and 100 µg/mL, respectively, compared to the THCPSi-SLNCs for the HepG2 cells; and ca. four- and 10-fold increase in the cellular associated fluorescence of the THCPSi nanoparticles at 50 and 100 µg/mL, respectively, compared to the THCPSi-SLNCs for the HT-29 cells.

The flow cytometry results were further corroborated with the confocal fluorescence microscope experiments, which were employed to evaluate the effect of the SLN matrix encapsulation on the cellular interactions of the THCPSi nanoparticles. In Figure 4, all the cells showed a normal morphology under the concentrations studied, indicating good cell viability and supporting the cell viability studies in Figure 3. Among all the three types of cells studied, more FITC-labelled THCPSi nanoparticles contacted with the cells than FITC-labelled THCPSi-SLNCs regardless of the concentration used (50 or 100 µg/mL; Figure 4a,b). When the concentration of the THCPSi nanoparticles increased to 100 µg/mL (Figure 4b), the cellular association for all the three types of studied cells was also greatly increased. In contrast, no significant differences on the amount of particles associated to all the three types of studied cells were observed when the concentration of the THCPSi-SLNCs was raised from 50 to 100 µg/mL. HT-29 cells are mucus secreting cells, and the association is believed to be more pronounced with these cells than with nonmucus secreting ones.[32] This was observed to be the case with the HT-29 cells and THCPSi nanoparticles. As for the THCPSi-SLNCs, no significant cellular association were observed with the HT-29 cells, unlike the protein-modified THCPSi nanoparticles previously reported.[32] From the confocal data it can also be observed that the THCPSi nanoparticles tend to aggregate more extensively, while no major aggregation was observed in the case of THCPSi-SLNCs when in contact with the cells.

Overall, the flow cytometry and the confocal fluorescence microscopy studies are in good agreement and showed that the THCPSi nanoparticles associated stronger to RAW 264.7, HepG2,

and HT-29 cells than the THCPSi-SLNCs in a concentration-dependent manner. Due to the instability of the THCPSi nanoparticles in the medium, they tend to aggregate and associate strongly with the cells. The results for the THCPSi-SLNCs can be attributed to the successful encapsulation of the THCPSi nanoparticles in the SLN matrix and the ability of the nanocomposite to minimize strong cell interactions due to its surface properties and higher stability, avoiding major particle aggregation, in particular with the RAW 264.7 macrophages, which can be regarded as advantageous for parenteral drug delivery. The reduction in the cellular interactions by the THCPSi-SLNCs seems to be even more remarkable than previously reported for protein-modified THCPSi nanoparticles.[32]

Since both THCPSi nanoparticles and THCPSi-SLNCs are negatively charged, it is unlikely that the different behavior in cellular association/interaction between them is a result of the particle charge. However, the surface roughness of the particles as well as the size of the particles may affect the cell–nanoparticle interactions.[23,24,43,44,52] Simulations of the nanoparticles interacting with synthetic membranes suggested that nanoscale surface roughness greatly minimizes repulsive interactions (e.g., electrostatic and hydrophilic), thereby promoting adhesion, which might translate into an easier interaction with the cells.[24,52] In addition, particles with hydrophobic surfaces are more readily interacting with the cell membrane than their less-hydrophobic counterparts.[52] After encapsulation, the THCPSi nanoparticles were trapped within the SLN matrix containing neutral polymers,[53] such as PEG and PVA, which simultaneously decreased the roughness and increased the size of the particles, enhancing the hydrophilicity of the THCPSi nanoparticles and maximized the repulsion interactions.[24] Consequently, this was translated into a decrease in the nanoparticle's association to cell membrane, particularly in the case of the macrophage cells, and an improvement in the cytocompatibility. In addition, the stronger cellular interactions observed for THCPSi nanoparticles in Figure 4 might result in high cell toxicity,[29,31–33,52] which was in good agreement with the cell viability data obtained in Figure 3.

2.4. Stability in Human Plasma

A very important prerequisite for an optimal nanocarrier is its stability in biological fluids.[52] Plasma protein adsorption onto the PSi can be affected by its surface modification with polymers or proteins.[29,34,35] The size, shape, surface charge, surface chemistry, surface topology, surface coating, and mechanical properties of the nanomaterials may also contribute significantly to the interaction with cells by affecting the ability of the nanomaterial to adsorb protein and/or altering the conformation of the adsorbed protein.[24,49,50,52–54] Bare THCPSi nanoparticles are prone to extensive aggregation when dispersed in water[29] due to their hydrophobic surface and also when added to human plasma due to their readily available large surface area for protein adsorption.[29] In order to further investigate the stability of the THCPSi-SLNCs in physiological conditions, both THCPSi nanoparticles and THCPSi-SLNCs were incubated in human plasma at 37 °C for 2 h (**Figure 5**).

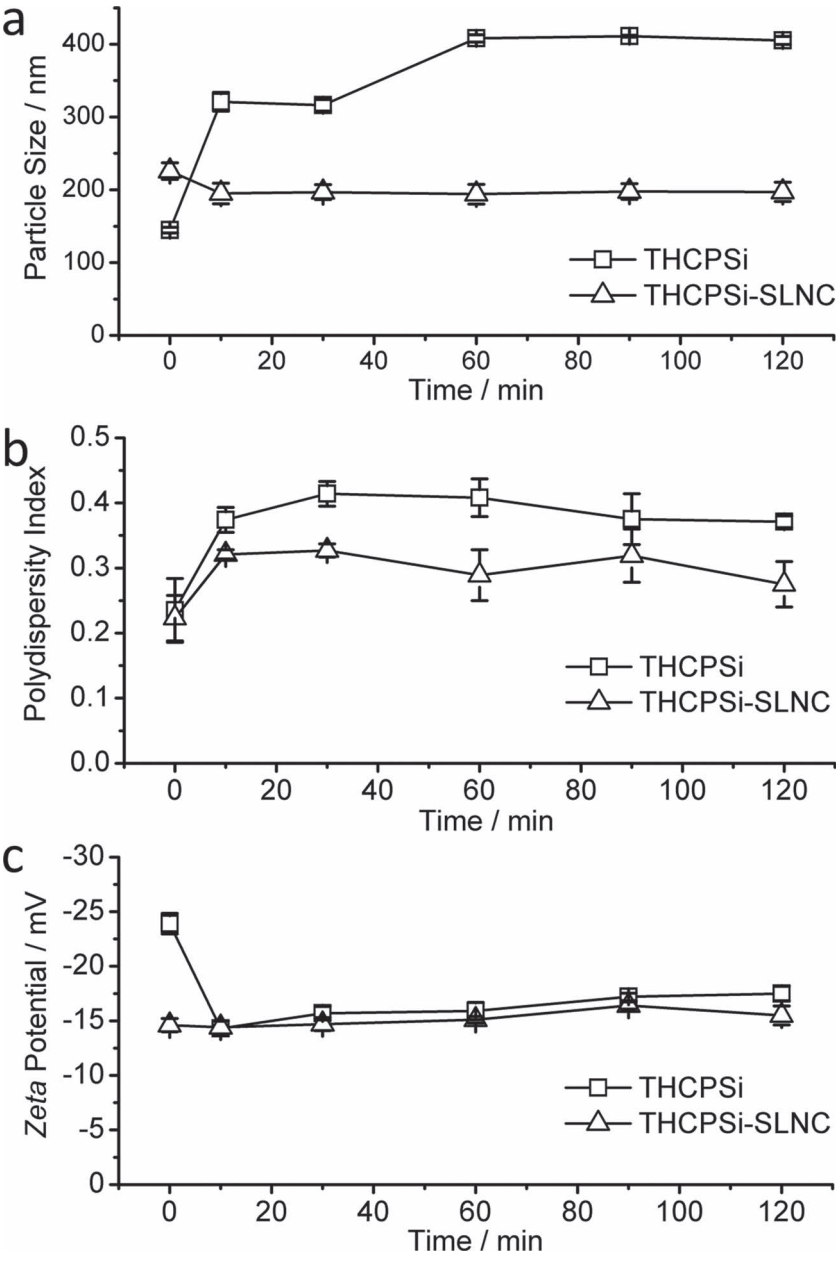

Figure 5. a) Impact of the human plasma on the particle size, b) polydispersity index (PDI), and c) ζ-potential for both the THCPSi nanoparticles and the THCPSi-SLNCs within 2 h incubation. The results were calculated from the light scattering measurement data as a function of time at 37 °C. Values denote the mean ± s.d. (n = 3).

Bare THCPSi nanoparticles were dispersed in 0.2% Tween 80/water solution (w/v) with tip-sonication and redispersed in water before incubation in human plasma.

The presence of Tween 80 slightly improved the stability of THCPSi nanoparticles (Figure 5a) compared to previous studies in absence of Tween 80.[29] Despite of that, the size of the THCPSi nanoparticles greatly increased from an average size of ca. 150 nm to ca. 320 nm after 10 min, and finally to an average size of ca. 400 nm after 2 h incubation in the plasma. In contrast, no aggregation was detected for the THCPSi-SLNCs after incubation in plasma and the average size of the particles remained unchanged at ca. 200 nm. This could be due to the different affinity of the plasma proteins to adsorb to the surface of the THCPSi-SLNCs compared to the bare nanoparticles.[29] As discussed above, the presence of the SLN matrix on the surface of THCPSi-SLNCs makes the hydrophobic surface of the THCPSi nanoparticles hydrophilic, which might be due to the hydrophilic components present in the SLN matrix. Furthermore, the great increase in the stability of the THCPSi-SLNCs can also be attributed to the presence of the polymers, PEG and PVA, on the nanocomposite's surface. In addition, both the surface smoothness improvement and the shape of the nanocomposite (Figure 1) could also decrease the protein adsorption onto the surface of the nanocomposites.[24] The polydispersity index (PDI) of both bare THCPSi nanoparticles and THCPSi-SLNCs increased after incubation with human plasma (Figure 5b), however the PDI increase was smaller for THCPSi-SLNCs than for the bare THCPSi nanoparticles.

The surface charge of the nanoparticles has also an important role on the protein–nanoparticle interactions and formation of protein corona,[24–26] therefore, the surface charge of the nanocomposite and the bare THCPSi nanoparticles were evaluated. The zeta (ζ)-potential of the THCPSi nanoparticles decreased from ca. −25 to −15 mV within the first 10 min after the incubation in plasma and remained unchanged after 2 h (Figure 5c). This effect was somehow expected because the ζ-potential of the THCPSi nanoparticles is likely to become more positive after an initial boost in the protein adsorption onto the nanoparticle's surface.[29] In the case of the THCPSi-SLNCs, the ζ-potential was constant at ca. −15 mV for the 2 h experiment. This demonstrates the lesser extent of plasma protein adsorption onto the surface of the nanocomposite due to more hydrophilic surface, and the presence of PEG and PVA polymers that can greatly maximize the repulsion interactions.[24] Although both THCPSi nanoparticles and THCPSi-SLNCs have a negative ζ-potential, the significant decrease of the ζ-potential in the bare THCPSi nanoparticles initially is mainly due to the immediate surface coverage by the plasma proteins and possible formation of nanoparticle–protein corona complexes.[25,26]

Overall, the plasma stability results demonstrate that the encapsulation of the THCPSi nanoparticles within the SLN matrix extensively hinders particle aggregation and minimizes protein adsorption.

2.5. Drug Loading and In Vitro Release

In order to evaluate the drug release profiles of the nanoparticles, a model drug was loaded into the THCPSi nanoparticles and THCPSi-SLNCs. Owing to the physicochemical properties, e.g., poor water-solubility and very low permeability (Biopharmaceutical Classification System Class IV), furosemide (FUR) was selected. The average loading degree for the FUR-loaded THCPSi nanoparticles (FUR-THCPSi) and the FUR-loaded THCPSi-SLNCs (FUR-THCPSi-SLNCs) obtained was ca. 21 and 15 wt%, respectively. The decrease in the drug loading degree for the FUR-THCPSi-SLNCs compared to the bare THCPSi ones is mainly due to the preparation method of the THCPSi-SLNCs. In this procedure the loaded THCPSi particles were immersed in oil phase during the emulsion process unlike the bare THCPSi nanoparticles. This could have led to a slightly decrease in the drug loading degree.

Three different buffer solutions with pH-values of 7.4, 5.5, and 1.2 were selected to simulate the pH under physiological conditions of the blood plasma and the gastrointestinal tract.[55] The release profiles of FUR-THCPSi nanoparticles and the FUR-THCPSi-SLNCs at different pH-values are shown in **Figure 6**. For both the THCPSi nanoparticles and the THCPSi-SLNCs, the FUR release rate decreased as the pH-values decreased. Regardless of the pH value, the FUR release rate from the THCPSi-SLNCs was always slower than that of bare THCPSi nanoparticles. At pH 7.4, more than 90% of drug was released within 1 h from the THCPSi nanoparticles and only ca. 40% from the THCPSi-SLNCs (Figure 6a). As the pH-value decreased to 5.5 (Figure 6b), only ca. 80% of FUR was released from the THCPSi nanoparticles within 1 h, whereas only ca. 15% of FUR released from the THCPSi-SLNCs. Furthermore, the FUR release was delayed from the particles at pH 1.2, reaching ca. 90% release from the THCPSi nanoparticles after ca. 8 h and ca. 55% from the nanocomposites for the same time (Figure 6c and inset). At both pH-values of 7.4 and 5.5, the FUR release from the THCPSi-SLNCs increased rather continuously over time, whereas for the THCPSi nanoparticles the FUR release showed an initial drug release burst followed by a continuous drug release. At pH 1.2, the FUR release from the THCPSi-SLNCs was constantly increased up to ca. 55% within 12.5 h, after which the release was steady over time. This could be partly ascribed to the significantly different properties and behavior of the phospholipid at low acidic pH-conditions, such as the increased phase transition temperature, gel-phase characteristics, and slightly alteration of phospholipid surface charge.[56,57]

The FUR release profiles in **Figure 6** are determined by the physicochemical properties of the drug (e.g., poor water-solubility)[58] and, most importantly, by the prepared nanocomposites. The in vitro release rate of FUR from the THCPSi nanoparticles was significantly slowed down after encapsulation within the SLN matrix. Moreover, the release data of FUR demonstrate that the SLN matrix played an important role in controlling the drug release from the THCPSi-SLNCs as well as in protecting the payload from premature release. This further corroborates the efficacy of the SLN matrix to encapsulate the THCPSi nanoparticles. The successful drug loading and release from the THCPSi-SLNCs also confirms that the THCPSi nanoparticles retained their structure after the encapsulation. The THCPSi-SLNCs are therefore very good candidates for controlling the drug release, particularly regarding prolonged drug release. This is of great importance for cancer therapy where the drug release should be controlled for better efficacy and safety reasons.[17]

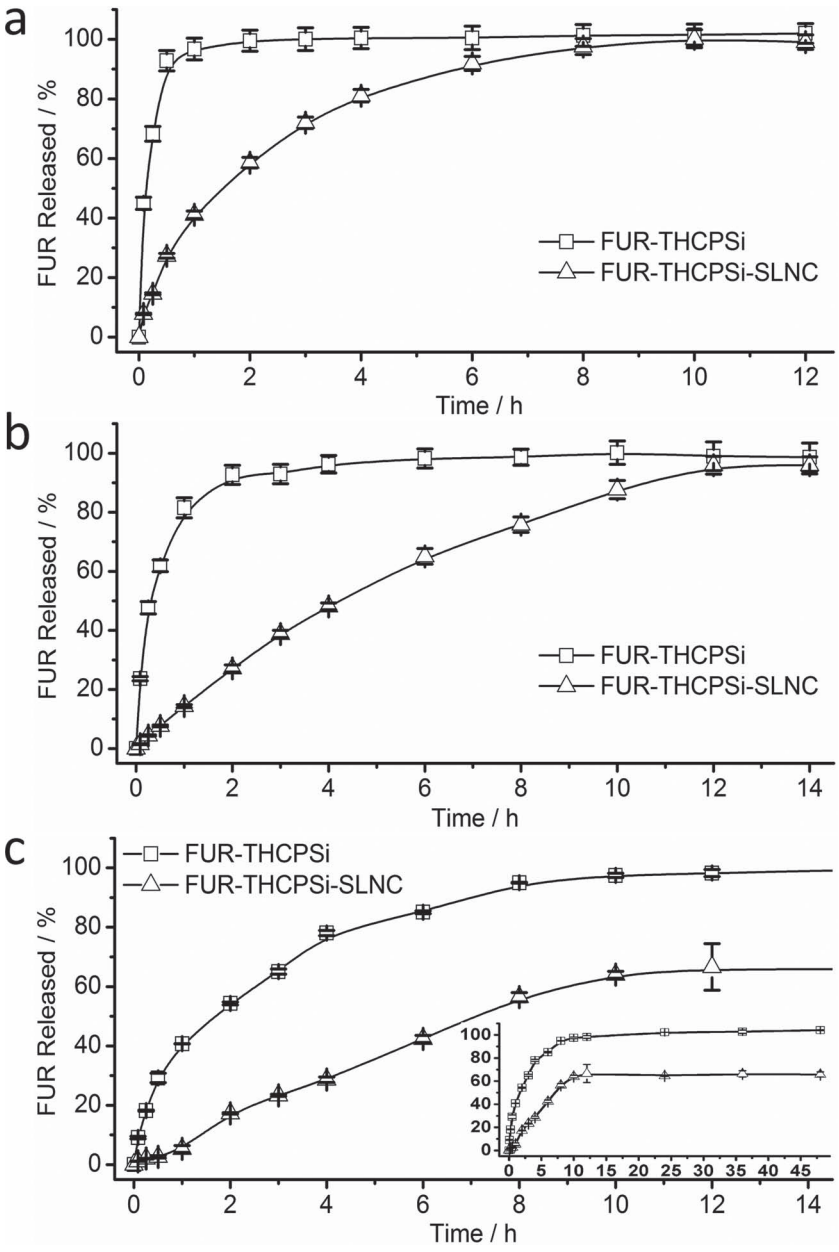

Figure 6. Release profiles of FUR-loaded THCPSi nanoparticles and FUR-loaded THCPSi-SLNCs at a) pH 7.4, b) pH 5.5, and c) pH 1.2. All experiments were conducted at 37 °C. Error bars represent the mean ± s.d. ($n = 3$).

3. Conclusions

In the present study, a novel class of THCPSi-SLNCs (on a 1:1 ratio) was produced by a S/O/W emulsion solvent evaporation method. TEM and FTIR studies showed successfully encapsulation of the THCPSi nanoparticles in the SLN matrix. The THCPSi-SLNCs changed the surface properties of the bare THCPSi nanoparticles, including its morphology and hydrophobicity. Furthermore, the nanocomposite provided several advantages over the bare nanoparticles and other existing nanodelivery systems, which include: (i) superior suspensibility and better stability against aggregation in aqueous solutions; (ii) increased particle smoothness; (iii) improved cytocompatibility, in particular with rather sensitive cell lines, such as RAW 264.7 macrophages; (iv) reduced cellular association and improved stability in human plasma in vitro, which should provide better protection against opsonization; and (v) prolonged drug delivery over a longer period of time, preventing the initial drug release burst. Our results suggest this nanocomposite as a promising candidate for targeting delivery applications. We are currently testing the in vivo efficacy of the THCPSi-SLNCs after intravenous administration to determine the effect of the SLN encapsulation on the circulation times and delivery of therapeutics to tumor cells.

4. Experimental Section

Production of THCPSi Nanoparticles: THCPSi nanoparticles were prepared by the electrochemical anodization method as described elsewhere.[5] Briefly, free-standing PSi multilayer films were anodized from boron doped p^+-type monocrystalline Si ⟨100⟩ wafers with a resistivity of 0.01–0.02 Ω cm using a 1:1 (v/v) aqueous HF (38%)-ethanol electrolyte. Following the hydrocarbonization treatment by exposing the PSi films to a flow of N_2 and acetylene (1:1, v/v), wet ball milling in 1-decene was employed to reduce the size of the THCPSi multilayer films while simultaneously minimizing the surface oxidation.[3,5] The final size sorting and change of the suspension media was achieved by centrifugation.

Preparation of THCPSi-SLNCs: A modified emulsion solvent evaporation method was used to prepare the THCPSi-SLNCs, similarly to the method used for the preparation of SLNs.[45] The only difference was the addition of the THCPSi nanoparticle suspension into the oil phase at the beginning of the preparation, a so-called solid-in-oil-in-water (S/O/W) emulsion solvent evaporation method.[36] Firstly, 100 mg of glycerol monosterate (GMS, VWR International, USA), 40 mg of L-α phosphatidylcholine (PC, Sigma-Aldrich, USA) and 200 µg of the THCPSi nanoparticles were dispersed into 5 mL ethanol at 70 °C forming the oil phase. Meanwhile, the aqueous phase, 15 mL of 1% polyvinyl alcohol (PVA, M_w 31–50 kDa, Sigma-Aldrich, USA) containing 1% polyethylene glycol 6000 (PEG 6000, Sigma-Aldrich, USA), was heated to the same temperature. The oil phase was then added into the aqueous phase drop-by-drop under vigorous stirring for dispersion. After the evaporation of ethanol, the hot emulsion was gradually dropped into 25 mL of 1% PVA containing 1% PEG 6000 under vigorous stirring at 2 °C to allow the solidification of the SLN matrix. The final suspension was sorted by centrifugation (Sorvall RC 5B Plus, Thermo Fisher Scientific, USA) at 15 000 rpm for 10 min to obtain the THCPSi-SLNCs. Fluorescein isothiocyanate (FITC, Sigma-Aldrich, USA)-labelled THCPSi nanoparticles were prepared by immersing the nanoparticles into a 100 µg/mL FITC ethanol solution for 2 h under stirring. FITC labelled-THCPSi nanoparticles were collected by centrifugation followed by 3 times washing with MilliQ-water to remove the excess of FITC. FITC-labelled THCPSi-SLNCs were obtained by adding 1000 µg of FITC and 200 µg of FITC labeled-THCPSi nanoparticles into 5 mL of organic phase during the nanocomposite preparation.

Characterization of THCPSi Nanoparticles and THCPSi-SLNCs: The physical properties of THCPSi nanoparticles were characterized by conducting N_2 sorption measurements at 77 K (Tristar 3000, Micromeritics Inc., USA). The specific surface area was calculated using the Brunauer–Emmett–Teller (BET) theory, whereas the pore volume and average diameter were obtained from the desorption branch of the isotherm using the Barrett–Joyner–Halenda (BJH) theory. The morphology of the THCPSi nanoparticles and the THCPSi-SLNCs were investigated by transmission electron microscopy (TEM, Tecnai F12, FEI Company, USA). The particle suspensions for TEM were diluted accordingly and then added onto the coated copper grids and allowed to dry for 24 h before the measurements. Due to the small size of THCPSi-SLNCs and the limited resolution of TEM to distinguish the encapsulated components, THCPSi-solid lipid composite microparticles were also studied under TEM. The chemical composition and interaction of the SLN matrix and the THCPSi nanoparticles was also studied with a Fourier transformed infrared spectroscopy (FTIR) instrument (Vertex 70, Bruker, USA), using a horizontal Attenuated Total Reflectance (ATR) accessory (MIRacle, PIKE Technologies, USA). The FTIR spectra were recorded in the wavelength region of 4000–650 cm^{-1} with a resolution of 4 cm^{-1} using OPUS 5.5 software at room temperature.

Cell Culture: The interaction of the cells with THCPSi nanoparticles and THCPSi-SLNCs were studied on RAW 264.7 (murine leukemic monocyte macrophage, passage numbers 23–26), HepG2 (human liver hepatocellular carcinoma, passage numbers 21–24) and HT-29 (human colon adenocarcinoma, passage numbers 28–32) cell lines (all from the American Type Culture Collection, USA). The HepG2 cells were cultured in Dulbecco's modified Eagle's medium (DMEM, EuroClone S.p.A., Italy) with 4.5 g/L glucose and 1% sodium pyruvate, supplemented with 10% FBS (Gibco, Invitrogen, USA), 1% nonessential amino acids, 1% L-glutamine, penicillin (100 IU/mL), and streptomycin (100 mg/mL) (all from EuroClone S.p.A.). The culture conditions of HT-29 and RAW 264.7 macrophages were similar with that of HepG2, but without sodium pyruvate. The cell cultures were maintained in a standard incubator (BB 16 gas, Heraeus Instruments GmbH, Germany) at 37 °C with an atmosphere of 5% CO_2 and 95% relative humidity. Prior to each test, the cells were harvested with 0.25% (v/v) trypsin–ethylenediamine tetraacetic acid–phosphate buffer saline (PBS).

Viability Assays: For the cell viability measurements, 100 µL of 5.0×10^5 cells/mL of HT-29, and 2.5×10^5 cells/mL of HepG2 and RAW 264.7 macrophage cells in DMEM suspension were seeded in 96-well plates (PerkinElmer Inc., USA) and allowed to attach for 24 h. The medium was aspirated and the wells were washed twice with fresh 1× Hanks balanced salt solution (HBSS, pH 7.4). Subsequently, 100 µL of THCPSi nanoparticle and THCPSi-SLNC suspensions with concentrations of 250, 100, 50, and 15 µg/mL were added into the wells. 1× HBSS (pH 7.4) and Triton X-100 were used as positive and negative controls, respectively. After 24 h incubation, the wells were washed once with 1× HBSS (pH 7.4) and the number of viable cells was assayed with CellTiter-Glo (Promega Corporation, USA) according to the manufacturer's instructions. The luminescence was measured on a Varioskan Flash fluorometer (Thermo Fisher Scientific, USA). All the assays were carried out at least in triplicate.

Flow Cytometry: Suspensions of RAW 264.7, HepG2 or HT-29 cells were seeded in 12-well plates at the concentration of 1.0×10^6 cells/mL. Following by 24 h of cell attachment to the wells, 50 and 100 µg/mL of FITC-labelled THCPSi nanoparticles and THCPSi-SLNCs were incubated with the cells for 3 h. After washing with HBSS (pH 7.4), the cells were harvested, and then fixed with 2% glutaraldehyde in PBS for 30 min at room temperature. Exactly 10 000 events were collected on a LSR II flow cytometer (BD Biosciences, USA) with a laser excitation wavelength of 488 nm using FACSDiva software. Untreated cells were employed as controls, and the background (due to the particles only) and debris were subtracted.

Confocal microscopy: Suspensions of 1×10^5 cells/mL of RAW 264.7, HepG2 or HT-29 cells were seeded in Lab-Tek Chamber Slides (Thermo Fisher Scientific, USA). After 24 h of cell attachment to the wells, 50 and 100 µg/mL of FITC-labelled THCPSi nanoparticles and FITC-labelled THCPSi-SLNCs were added into the wells. Following by 3 h incubation, the particles were removed and the wells were washed three times with HBSS (pH 7.4). CellMask with a concentration of 5 µg/mL was added for cell staining according to the manufacturer specifications. Prior to the measurements, the cells were fixed with 2.5% glutaraldehyde in PBS for 30 min at room temperature. Confocal images were taken with a Leica SP2 inverted confocal microscope, equipped with argon (488 nm) and DPSS (561 nm) lasers, and using a HCX Plan Apochromat 63/1.2-0.6 oil immersion objective (Leica Microsystems, Germany).

Human Plasma Stability Studies: To determine the impact of the SLN matrix on the stability of the PSi particles, the THCPSi nanoparticles and THCPSi-SLNCs were incubated with human plasma at 37 ± 1 °C for 2 h. Samples were withdrawn at different time intervals and diluted several times with water before the average particle size and average ζ-potential measurements (Zetasizer Nano ZS, Malvern Instruments, UK). Anonymous donor human plasma was obtained from the Finnish Red Cross Blood Service.

Drug Loading and Release Experiments: Furosemide (FUR)-loaded THCPSi (FUR-THCPSi) nanoparticle samples were obtained by immersing the nanoparticles into a 20 mg/mL of FUR acetone solution with a ratio of ca. 1:1 (w/w) and stirring for 2 h. FUR-THCPSi nanoparticles were collected by centrifugation following by 3 times washing with MilliQ-water to remove the excess of unloaded FUR. FUR-loaded THCPSi-SLNCs (FUR-THCPSi-SLNCs) were obtained by adding 20 mg FUR and 200 µg unwashed FUR-THCPSi nanoparticles into 5 mL oil phase during the nanocomposite preparation. FUR-THCPSi-SLNCs were also washed twice with MilliQ-water before the loading degree determination and the release experiment to remove the free FUR. The loading degree of FUR was determined by immersing the FUR-THCPSi nanoparticle and FUR-THCPSi-SLNCs samples in methanol for 24 h. The amount of FUR released from the particles was determined by HPLC using an Agilent 1260 (Agilent Technologies, USA). The HPLC mobile phase was composed of 10 mM sodium citrate buffer (pH 5.5) and acetonitrile (ratio of 70:30, v/v), the flow rate was 1.0 mL/min, the wavelength used for FUR quantification was 234 nm and the temperature was set at 30 °C. A Discover C18 column (4.6 mm × 150 mm, 5 µm, Supelco Analytical, USA) was used as stationary phase and the sample injection volume was 20 µL. The in vitro release profiles of FUR from the THCPSi nanoparticles and THCPSi-SLNCs were made in a dialysis diffusion bag (T1, Cellu Sep, USA). Firstly, 1000 µg of THCPSi nanoparticles and ca. 3000 µg of THCPSi-SLNCs containing 1000 µg of THCPSi nanoparticles were added into the dialysis diffusion bags. The amount of FUR loaded was ca. 300 µg and ca. 500 µg for THCPSi nanoparticles and THCPSi-SLNCs, respectively. Then, the release of FUR was measured by immersing the dialysis diffusion bags in 250 mL of buffer solutions with pH 1.2 (0.2 M NaCl + 0.2 M HCl), pH 5.5 (HBSS–MES) and pH 7.4 (HBSS–HEPES), using a shaking method with a stirring speed rate of 100 rpm at 37 ± 1 °C. Samples of 1.0 mL were withdrawn at different time points, and 1.0 mL of preheated release media was added to replace the withdrawn volume. After sampling, the aliquots were centrifuged for 1 min at 12 000 rpm and the FUR concentration quantified by HPLC as described above.

Statistical Analyses: Results from several tests are expressed as the mean ± s.d. for at least three independent experiments. A one-way analysis of variance (ANOVA), followed by a Student's *t*-test was employed to analyse the data. The analysis was carried out using Origin 7.5 SR7 (OriginLab Corp., UK) and the level of significance was set at a probability of $^{*}p < 0.05$ and $^{**}p < 0.01$.

Supporting Information

Supporting Information is available from the Wiley Online Library or from the author.

Acknowledgements

H.A.S. acknowledges financial support from the Academy of Finland (decision numbers 252215 and 256394). We thank Dr. Anu Airaksinen (Laboratory of Radiochemistry, Department of Chemistry, University of Helsinki, Finland) for technical support with the Zetasizer instrument and Dr. Luis M. Bimbo for technical support with Varioskan. Prof. Bruno Sarmento (Department of Pharmaceutical Technology, University of Porto, Portugal) and Dr. Yanru Lou (Division of Biopharmaceutics and

Pharmacokinetics, University of Helsinki, Finland) are acknowledged for generously providing the HT-29 and the HepG2 cell lines, respectively.

Received: August 30, 2012
Revised: October 9, 2012
Published online: November 6, 2012

[1] H. A. Santos, L. M. Bimbo, V. P. Lehto, A. J. Airaksinen, J. Salonen, J. Hirvonen, *Curr. Drug Discovery Technol.* **2011**, *8*, 228.
[2] J. Salonen, L. Laitinen, A. M. Kaukonen, J. Tuura, M. Bjorkqvist, T. Heikkila, K. Vaha-Heikkila, J. Hirvonen, V. P. Lehto, *J. Controlled Release* **2005**, *108*, 362.
[3] J. Salonen, A. M. Kaukonen, J. Hirvonen, V. P. Lehto, *J. Pharm. Sci.* **2008**, *97*, 632.
[4] R. E. Serda, B. Godin, E. Blanco, C. Chiappini, M. Ferrari, *Biochim. Biophys. Acta* **2011**, *1810*, 317.
[5] L. M. Bimbo, M. Sarparanta, H. A. Santos, A. J. Airaksinen, E. Makila, T. Laaksonen, L. Peltonen, V. P. Lehto, J. Hirvonen, J. Salonen, *ACS Nano* **2010**, *4*, 3023.
[6] S. P. Low, N. H. Voelcker, L. T. Canham, K. A. Williams, *Biomaterials* **2009**, *30*, 2873.
[7] T. Tanaka, B. Godin, R. Bhavane, R. Nieves-Alicea, J. Gu, X. Liu, C. Chiappini, J. R. Fakhoury, S. Amra, A. Ewing, Q. Li, I. J. Fidler, M. Ferrari, *Int. J. Pharm.* **2010**, *402*, 190.
[8] H. Jaganathan, B. Godin, *Adv. Drug Delivery Rev.* **2012**, DOI: 10.1016/j.addr.2012.05.008.
[9] E. Tasciotti, X. W. Liu, R. Bhavane, K. Plant, A. D. Leonard, B. K. Price, M. M. C. Cheng, P. Decuzzi, J. M. Tour, F. Robertson, M. Ferrari, *Nat. Nanotechnol.* **2008**, *3*, 151.
[10] M. Kilpelainen, J. Riikonen, M. A. Vlasova, A. Huotari, V. P. Lehto, J. Salonen, K. H. Herzig, K. Jarvinen, *J. Controlled Release* **2009**, *137*, 166.
[11] P. Kinnari, E. Mäkilä, T. Heikkilä, J. Salonen, J. Hirvonen, H. A. Santos, *Int. J. Pharm.* **2011**, *414*, 148.
[12] M. Tahvanainen, T. Rotko, E. Makila, H. A. Santos, D. Neves, T. Laaksonen, A. Kallonen, K. Hamalainen, M. Peura, R. Serimaa, J. Salonen, J. Hirvonen, L. Peltonen, *Int. J. Pharm.* **2012**, *422*, 125.
[13] L. M. Bimbo, E. Makila, T. Laaksonen, V. P. Lehto, J. Salonen, J. Hirvonen, H. A. Santos, *Biomaterials* **2011**, *32*, 2625.
[14] M. Kilpelainen, J. Monkare, M. A. Vlasova, J. Riikonen, V. P. Lehto, J. Salonen, K. Jarvinen, K. H. Herzig, *Eur. J. Pharm. Biopharm.* **2011**, *77*, 20.
[15] T. Tanaka, L. S. Mangala, P. E. Vivas-Mejia, R. Nieves-Alicea, A. P. Mann, E. Mora, H. D. Han, M. M. Shahzad, X. Liu, R. Bhavane, J. Gu, J. R. Fakhoury, C. Chiappini, C. Lu, K. Matsuo, B. Godin, R. L. Stone, A. M. Nick, G. Lopez-Berestein, A. K. Sood, M. Ferrari, *Cancer Res.* **2010**, *70*, 3687.
[16] J. W. Liu, X. M. Jiang, C. Ashley, C. J. Brinker, *J. Am. Chem. Soc.* **2009**, *131*, 7567.
[17] L. M. Bimbo, L. Peltonen, J. Hirvonen, H. A. Santos, *Curr. Drug Metab.* **2012**, *13*, 1068.
[18] Q. Sun, M. Radosz, Y. Shen, *J. Controlled Release* **2012**, DOI:10.1016/j.jconrel.2012.05.042.
[19] R. K. Jain, T. Stylianopoulos, *Nat. Rev. Clin. Oncol.* **2010**, *7*, 653.
[20] E. J. Anglin, L. Y. Cheng, W. R. Freeman, M. J. Sailor, *Adv. Drug Delivery Rev.* **2008**, *60*, 1266.
[21] J. Wu, M. J. Sailor, *Adv. Funct. Mater.* **2009**, *19*, 733.
[22] J. R. Dorvee, M. J. Sailor, G. M. Miskelly, *Dalton Trans.* **2008**, *6*, 721.
[23] P. P. Karmali, D. Simberg, *Expert Opin. Drug Deliv.Delivery* **2011**, *8*, 343.
[24] M. Mahmoudi, I. Lynch, M. R. Ejtehadi, M. P. Monopoli, F. B. Bombelli, S. Laurent, *Chem. Rev.* **2011**, *111*, 5610.
[25] T. Cedervall, I. Lynch, S. Lindman, T. Berggard, E. Thulin, H. Nilsson, K. A. Dawson, S. Linse, *Proc. Natl. Acad. Sci. USA* **2007**, *104*, 2050.
[26] I. Lynch, A. Salvati, K. A. Dawson, *Nat. Nanotechnol.* **2009**, *4*, 546.
[27] D. A. Barrett, M. S. Hartshorne, M. A. Hussain, P. N. Shaw, M. C. Davies, *Anal. Chem.* **2001**, *73*, 5232.
[28] J. M. Harris, R. B. Chess, *Nat. Rev. Drug Discovery* **2003**, *2*, 214.
[29] M. Sarparanta, L. M. Bimbo, J. Rytkonen, E. Makila, T. J. Laaksonen, P. Laaksonen, M. Nyman, J. Salonen, M. B. Linder, J. Hirvonen, H. A. Santos, A. J. Airaksinen, *Mol. Pharmaceutics* **2012**, *9*, 654.
[30] M. Sarparanta, E. Makila, T. Heikkila, J. Salonen, E. Kukk, V. P. Lehto, H. A. Santos, J. Hirvonen, A. J. Airaksinen, *Mol. Pharmaceutics* **2011**, *8*, 1799.
[31] M. P. Sarparanta, L. M. Bimbo, E. M. Makila, J. J. Salonen, P. H. Laaksonen, A. M. Helariutta, M. B. Linder, J. T. Hirvonen, T. J. Laaksonen, H. A. Santos, A. J. Airaksinen, *Biomaterials* **2012**, *33*, 3353.
[32] L. M. Bimbo, M. Sarparanta, E. Makila, T. Laaksonen, P. Laaksonen, J. Salonen, M. B. Linder, J. Hirvonen, A. J. Airaksinen, H. A. Santos, *Nanoscale* **2012**, *4*, 3184.
[33] L. M. Bimbo, E. Makila, J. Raula, T. Laaksonen, P. Laaksonen, K. Strommer, E. I. Kauppinen, J. Salonen, M. B. Linder, J. Hirvonen, H. A. Santos, *Biomaterials* **2011**, *32*, 9089.
[34] J. H. Park, L. Gu, G. von Maltzahn, E. Ruoslahti, S. N. Bhatia, M. J. Sailor, *Nat. Mater.* **2009**, *8*, 331.
[35] L. S. Wang, L. C. Wu, S. Y. Lu, L. L. Chang, I. T. Teng, C. M. Yang, J. A. A. Ho, *ACS Nano* **2010**, *4*, 4371.
[36] D. M. Fan, E. De Rosa, M. B. Murphy, Y. Peng, C. A. Smid, C. Chiappini, X. W. Liu, P. Simmons, B. K. Weiner, M. Ferrari, E. Tasciotti, *Adv. Funct. Mater.* **2012**, *22*, 282.
[37] C. E. Ashley, E. C. Carnes, G. K. Phillips, D. Padilla, P. N. Durfee, P. A. Brown, T. N. Hanna, J. Liu, B. Phillips, M. B. Carter, N. J. Carroll, X. Jiang, D. R. Dunphy, C. L. Willman, D. N. Petsev, D. G. Evans, A. N. Parikh, B. Chackerian, W. Wharton, D. S. Peabody, C. J. Brinker, *Nat. Mater.* **2011**, *10*, 389.
[38] R. H. Muller, R. Shegokar, C. M. Keck, *Curr. Drug Discovery Technol.* **2011**, *8*, 207.
[39] W. Mehnert, K. Mader, *Adv. Drug Delivery Rev.* **2001**, *47*, 165.
[40] A. J. Almeida, E. Souto, *Adv. Drug Delivery Rev.* **2007**, *59*, 478.
[41] I. P. Kaur, R. Bhandari, S. Bhandari, V. Kakkar, *J. Controlled Release* **2008**, *127*, 97.
[42] M. L. Bondi, E. F. Craparo, G. Giammona, F. Drago, *Nanomedicine* **2010**, *5*, 25.
[43] P. V. AshaRani, G. Low Kah Mun, M. P. Hande, S. Valiyaveettil, *ACS Nano* **2009**, *3*, 279.
[44] W. Jiang, B. Y. Kim, J. T. Rutka, W. C. Chan, *Nat. Nanotechnol.* **2008**, *3*, 145.
[45] D. F. Liu, S. M. Jiang, H. Shen, S. Qin, J. J. Liu, Q. Zhang, R. Li, Q. W. Xu, *J. Nanopart. Res.* **2011**, *13*, 2375.
[46] A. Manosroi, P. Wongtrakul, J. Manosroi, H. Sakai, F. Sugawara, M. Yuasa, M. Abe, *Colloids Surf., B* **2003**, *30*, 129.
[47] H. A. Santos, J. Riikonen, J. Salonen, E. Makila, T. Heikkila, T. Laaksonen, L. Peltonen, V. P. Lehto, J. Hirvonen, *Acta Biomater.* **2010**, *6*, 2721.
[48] I. Canton, G. Battaglia, *Chem. Soc. Rev.* **2012**, *41*, 2718.
[49] K. Saha, A. Bajaj, B. Duncan, V. M. Rotello, *Small* **2011**, *7*, 1903.
[50] A. Kumari, S. K. Yadav, *Expert Opin. Drug Delivery* **2011**, *8*, 141.
[51] S. E. Gratton, P. A. Ropp, P. D. Pohlhaus, J. C. Luft, V. J. Madden, M. E. Napier, J. M. DeSimone, *Proc. Natl. Acad. Sci. USA* **2008**, *105*, 11613.
[52] A. E. Nel, L. Madler, D. Velegol, T. Xia, E. M. V. Hoek, P. Somasundaran, F. Klaessig, V. Castranova, M. Thompson, *Nat. Mater.* **2009**, *8*, 543.
[53] A. Verma, F. Stellacci, *Small* **2010**, *6*, 12.
[54] E. C. Cho, J. W. Xie, P. A. Wurm, Y. N. Xia, *Nano Lett.* **2009**, *9*, 1080.
[55] D. Schmaljohann, *Adv. Drug Delivery Rev.* **2006**, *58*, 1655.
[56] Y. Zhou, R. M. Raphael, *Biophys. J.* **2007**, *92*, 2451.
[57] H. Trauble, H. Eibl, *Proc. Natl. Acad. Sci. USA* **1974**, *71*, 214.
[58] G. E. Granero, M. R. Longhi, M. J. Mora, H. E. Junginger, K. K. Midha, V. P. Shah, S. Stavchansky, J. B. Dressman, D. M. Barends, *J. Pharm. Sci.* **2010**, *99*, 2544.